AD-A016 673

IONOSPHERIC EFFECTS INDUCED BY PRECIPITATING AURORAL
ELECTRONS. HAES REPORT NUMBER 14

J. B. Cladis, et al

Lockheed Missiles and Space Company, Incorporated

Prepared for:

Defense Nuclear Agency

22 July 1975

YC

314169

DNA 3648F

IONOSPHERIC EFFECTS INDUCED BY PRECIPITATING AURORAL ELECTRONS

HAES Report No. 14

ADA016673

Lockheed Missiles and Space Company, Inc.
3251 Hanover Street
Palo Alto, California 94304

22 July 1975
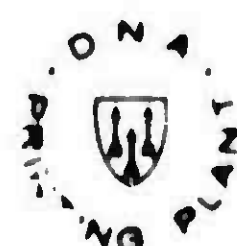
Final Report for Period 1 February 1974—1 February 1975

CONTRACT No. DNA 001-74-C-0146

APPROVED FOR PUBLIC RELEASE;
DISTRIBUTION UNLIMITED.

Prepared for

Director

DEFENSE NUCLEAR AGENCY

Washington, D. C. 20305

Destroy this report when it is no longer
needed. Do not return to sender.

REPORT DOCUMENTATION PAGE		READ INSTRUCTIONS BEFORE COMPLETING FORM
1. REPORT NUMBER DNA 3648F	2. GOVT ACCESSION NO.	3. RECIPIENT'S CATALOG NUMBER
4. TITLE (and Subtitle) IONOSPHERIC EFFECTS INDUCED BY PRECIPITATING AURORAL ELECTRONS HAES Report No. 14		5. TYPE OF REPORT & PERIOD COVERED Final Report for Period 1 Feb 74 —1 Feb 75
		6. PERFORMING ORG. REPORT NUMBER
7. AUTHOR(s) J. B. Cladis, G. T. Davidson, W. E. Francis L. L. Newkirk, M. Walt		8. CONTRACT OR GRANT NUMBER(s) DNA 001-74-C-0146
9. PERFORMING ORGANIZATION NAME AND ADDRESS Lockheed Missiles and Space Company, Inc. 3251 Hanover Street Palo Alto, California 94304		10. PROGRAM ELEMENT, PROJECT, TASK AREA & WORK UNIT NUMBERS NWET Subtask L25AAXYX966-14
11. CONTROLLING OFFICE NAME AND ADDRESS Director Defense Nuclear Agency Washington, D.C. 20305		12. REPORT DATE 22 July 1975
		13. NUMBER OF PAGES 46
14. MONITORING AGENCY NAME & ADDRESS(if different from Controlling Office)		15. SECURITY CLASS. (of this report) UNCLASSIFIED
		15a. DECLASSIFICATION/DOWNGRADING SCHEDULE

16. DISTRIBUTION STATEMENT (of this Report)

Approved for public release; distribution unlimited.

17. DISTRIBUTION STATEMENT (of the abstract entered in Block 20, if different from Report)

18. SUPPLEMENTARY NOTES

This work sponsored by the Defense Nuclear Agency under
Subtask L25AAXY966-14.

19. KEY WORDS (Continue on reverse side if necessary and identify by block number)

Auroral Electrons
Trapped Particles
Particle Precipitation in Atmosphere

Ionospheric Irregularities
Plasma Instabilities
AURORA Computer Code

20. ABSTRACT (Continue on reverse side if necessary and identify by block number)

The results of a coordinated experiment conducted in the auroral zone on 8 December 1971 were used to determine whether the AURORA computer code includes all of the important processes associated with the precipitation of electrons in the atmosphere. A precipitating electron flux was measured with the 1971-089A satellite simultaneously with ionospheric electron number-density distribution measurements using the Chatanika incoherent-scatter radar. The electron density distribution was compared with the distribution computed by the

DD FORM 1473 EDITION OF 1 NOV 65 IS OBSOLETE

20. ABSTRACT (Continued)

AURORA code, using the measured electron flux as input. Within the accuracy of the experiment, the computed and observed distributions were in agreement.

A meeting was organized to review the elements of various codes that are being used for DNA programs to compute atmospheric conditions resulting from precipitating electrons. The results of two test problems that were computed by the separate codes and presented at the meeting are discussed.

The AURORA code was utilized to compute energy-deposition profiles in the atmosphere due to the precipitation of electrons released by high-altitude nuclear detonations. These data were distributed to the Systems Code community for use in radar and IR systems codes.

The low-energy limit of the Aurora code was extended from 500 eV to about 1 eV by incorporating a code developed at UCSD. This low-energy portion of the code has also been extensively modified to eliminate computational oscillations and to improve its running efficiency, accuracy, and reliability.

The precipitation rate of relativistic electrons produced by a high-altitude nuclear explosion was found to be susceptible to alteration by an electron-ion-cyclotron wave instability. It was found that finite-temperature effects limit the instability to electrons with energies in the MeV range, but the growth rates for those electrons were found to be large.

PREFACE

The High Altitude Effects Simulation (HAES) Program sponsored by the Defense Nuclear Agency since the early 1970 time period, comprises several groupings of separate, but interrelated technical activities, e.g., ICECAP (Infrared Chemistry Experiments-Coordinated Auroral Program). Each of the latter have the common objective of providing information ascertained as essential for the development and validation of predictive computer codes designed for use with high priority DoD radar, communications, and optical defensive system.

Since the inception of the HAES Program, significant achievements and results have been described in reports published by DNA, participating service laboratories, and supportive organizations. In order to provide greater visibility for such information and enhance its timely applications, significant reports published since early calendar 1974 shall be identified with an assigned HAES serial number and the appropriate activity acronym (e.g., ICECAP) as part of the report title. A complete and current bibliography of all HAES reports issued prior to and subsequent to HAES Report No. 1, dated 5 February 1974 entitled, "Rocket Launch of an SWIR Spectrometer into an Aurora (ICE CAP 72)," AFCRL Environmental Research Paper No. 466, is maintained and available on request from DASIAC, DoD Nuclear Information and Analysis Center, 816 State Street, Santa Barbara, California 93102, Telephone (805) 965-0551.

This report, which is the final report under DNA contract 001-74-C-0146 is the fourteenth report in the HAES series and covers technical activities performed during the period February 1974 through February 1975. Portions of this program were reported previously in DNA Report 3293F entitled "ICECAP

1

Analysis: Mechanisms for Energy Deposit in the Auroral Ionosphere;" in DNA Report 3566F entitled "ICECAP Analysis: Energy Deposit and Transport in the Auroral Ionosphere;" and in other reports listed in the HAES bibliography and pre-HAES bibliography. The purpose of the work reported herein was to investigate the importance of various high-altitude energy input and transport mechanisms of interest to ICECAP experiments; to provide empirical quantitative models of these processes as the data allow; to assist in ICECAP data interpretation; and to assist in planning and execution of the ICECAP program.

TABLE OF CONTENTS

LIST OF ILLUSTRATIONS

1. INTRODUCTION

A high-altitude nuclear explosion (HANE) greatly disturbs the ionosphere-magnetosphere system, enhancing the excitation, ionization and temperature of the upper atmosphere, producing new chemical species, causing plasma irregularities, and storing in the magnetosphere a long-term source of highly-ionizing radiation. The attendant emissions in the infrared, visible, and ultraviolet interfere with missile-tracking devices. The enhanced ionization, especially in the irregularities, affects communications, radar, and navigation systems. It is therefore important to predict the conditions that would ensue in the event of a HANE and to determine the effects on operational systems.

One of the most important considerations is the distribution of the ionization in the atmosphere produced by the relativistic electrons released by a nuclear detonation. The AURORA code has been developed at LMSC to treat this problem. The code includes the effects of collisions and the converging magnetic field. The computations have been verified by laboratory experiments and by geophysical observations at relatively low L values where collision effects in the atmosphere are clearly dominant processes. However, in the auroral zone, as in the case of a HANE, additional processes such as plasma instabilities and electric fields may affect the motions of the precipitating electrons. It is therefore important to determine the importance of these processes. Accordingly, several tests of this code have been made utilizing the results of coordinated experiments wherein the precipitation electrons were observed with a low-altitude satellite and the distribution of the electron number density in the atmosphere, resulting from the incident electrons, was measured with the Chatanika incoherent scatter radar. Results of one test were presented in a previous report (Ref. 1). New results on a second case are described in Section 2. In every case the ionization profile computed by the code was in agreement with the experimental data, within the accur-

acies of the pertinent parameters. However, the experiments were not sufficiently precise to provide a definitive test of the code.

Several independently-developed codes are now in use on DNA programs to compute atmospheric effects of precipitating electrons. A meeting was therefore organized to discuss the elements of the codes and to compare the results computed by the codes for the same test problems. The data presented at the meeting are discussed in Section 3.

Some new applications of the AURORA code involving the precipitation of fission-decay electrons in the atmosphere are also discussed in Section 3.

Recently, the original version of the UCSD code (see Section 4) was incorporated in the AURORA code to compute electron fluxes in the energy range 1 - 500 eV (primaries and secondaries) that result from the interactions of precipitating electrons with the atmospheric constituents. This low-energy portion of the code has been revised, as discussed in Section 4, and can now be reliably applied to problems involving various chemical-reaction rates, atomic-excitation rates, and optical-emission rates.

Finally, in Section 5 a wave-particle instability is discussed which may seriously affect the distribution of the trapped electrons ensuing from a nuclear detonation. Among other effects, the instability could cause rapid pitch-angle diffusion of the electrons at relatively low altitudes, and thereby modify the ionization profiles predicted by the existing computer codes.

2. ANALYSIS OF THE COORDINATED EXPERIMENT IN AURORAL ZONE

In a previous study (Ref. 1), we utilized the existing data from a coordinated radar-satellite experiment (January 27, 1972) to test whether the AURORA code includes all important theoretical processes required to calculate correct auroral electron energy deposition rates in the atmosphere. The experiment involved the DNA incoherent-scatter radar at Chatanika, Alaska (Ref. 2) and the polar-orbiting satellite 1971-089A (Ref. 3).

The results obtained in that investigation indicated that the theory incorporated in AURORA is adequate to account for auroral electron energy deposition rates in the atmosphere. However, due to the large experimental uncertainties and the poor radar-satellite geometry associated with that case, it was recognized that additional cases must be investigated in order to obtain a more conclusive result.

We have recently investigated another case employing data from a radar-satellite experiment conducted near 1331 UT on 8 December 1971. The same analytic procedure described in Reference 1 was used to analyze these data.

Only the high-energy (> 500 eV) part of the AURORA code was used in this investigation. The effects due to the modification of the low-energy part of the code are discussed in Section 4. The contribution to electron energy deposition rates below 500 eV were estimated by extrapolation of the AURORA results into this region. The correction amounted to only ~ 5 percent in the region of the peak, and ~ 10 percent at higher altitudes.

It will be recalled that the high-energy code numerically solves the appropriate Fokker-Planck, steady-state diffusion equation to determine the flux of electrons produced in the atmosphere by a given spectrum of incident auroral electrons. The solution takes into account atmospheric scattering, electron energy loss, and the

9

mirroring effect of the geomagnetic field. The rate at which energy is deposited in the atmosphere by electrons is also calculated by the program.

In the coordinated radar-satellite experiment, particle detectors on the satellite measured the incident flux of auroral electrons at the satellite altitude. Simultaneously, radar measurements were made to determine the electron number density altitude profile produced in the E-region by the incident electrons interacting with atmospheric particles. To test the accuracy of the program, this experimental E-region electron density profile is compared with the theoretically predicted profile derived from electron energy deposition rates calculated by AURORA for the measured incident auroral electron flux. The theoretical profile is determined from the equation $N = \sqrt{q/\alpha}$ that expresses the balance between electron production and loss in the E-region. N is the electron number density, α is the effective recombination coefficient, and q is the ion-pair production rate produced by the auroral electrons. All three quantities are a function of altitude. Available experimental values of α pertaining to the auroral zone are used in the equation for N, and are given in Ref. 1. They are also shown in Figure 1. Values of q are determined from energy deposition rates (eV/cm^3/sec) obtained from AURORA after division by 35 eV/ion pair.

Figure 2 shows a plan view of the geometry between the radar beam (azimuth = 279°, elevation = 68°) and the satellite trajectory at 795 km altitude mapped down geomagnetic field lines to 110 km altitude, the altitude region of major interest. The radar beam and the field line through the satellite position at 1331:09 UT intersect the indicated altitudes at the locations shown. Precipitating auroral electrons tend to lie along lines of constant geomagnetic latitude. The line of constant geomagnetic latitude passing through the radar region of measurement at 110 km altitude would intersect the satellite trace approximately halfway between

10

EFFECTIVE RECOMBINATION COEFFICIENT (CM³ SEC⁻¹)

ALTITUDE (KM)

○ OMHOLT (REF. 4); POPOFF ET AL. (REF. 5)
□ MEYEROTT AND EVANS (REF. 6)
● JOHNSON AND BRADBURY (REF. 7); POPOFF ET AL. (REF. 5)
▽ JESPERSON ET AL. (REF. 8)
◇ ◁ ▷ ULWICK (REF. 9)
▼ ■ MCDIARMAD AND BUDZINSKI (REF. 10)
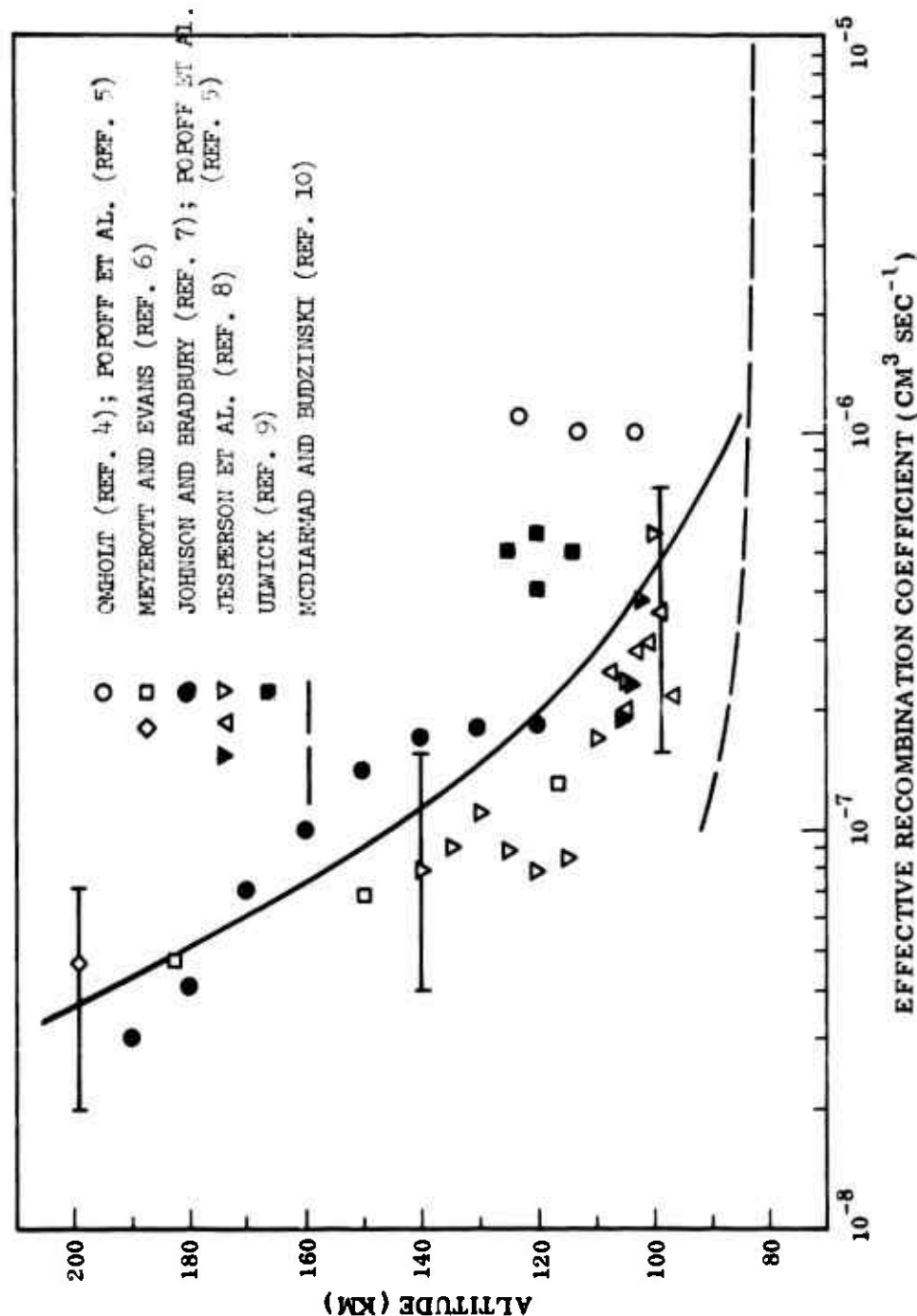
Figure 1 Experimental values of the effective recombination coefficient α. Omholt's values were revised by Popoff et al. (Ref. 5) using a more recent value of к= 12.5 for the ratio of total electron production to the total N₂⁺ first negative band system. The revised values are shown. Johnson and Bradbury revised their preliminary values of α (Ref. 7) which are published in Meyerott and Evans (Ref.6). Their revised values, which are reported by Popoff et al. (Ref.5), are plotted here.

11
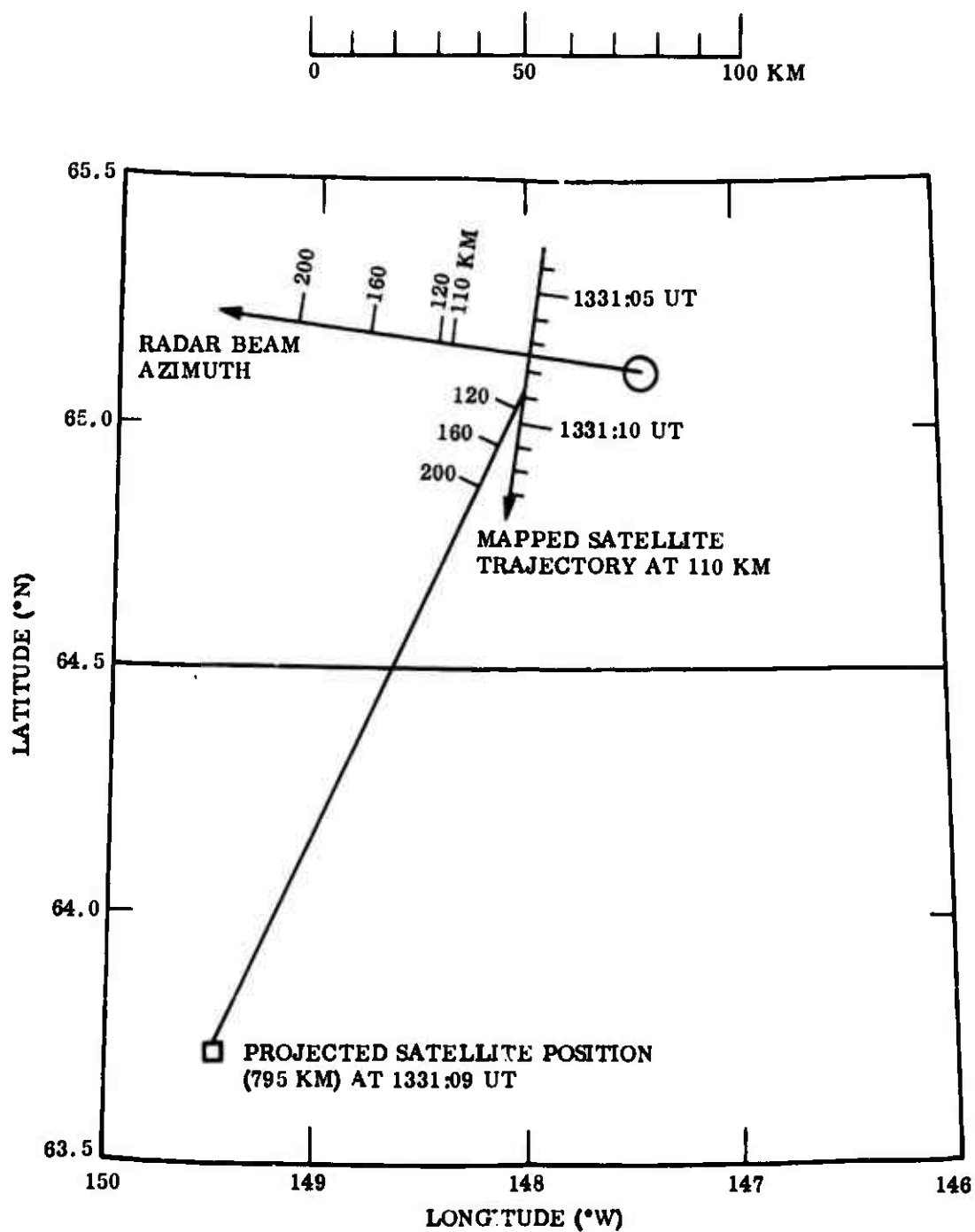
Figure . Plan view geometry of the radar beam and the mapped satellite trajectory during the coordinated experiment conducted at Chatanika, Alaska on 8 December 1971.

the 8-sec and 9-sec marks. Figure 2 indicates that at E-region heights the region of radar measurements is separated by distances of 20-40 km from the region of precipitating electrons beneath the satellite. Thus, in order to compare results in these two regions, as we do, we must assume that the characteristics of the precipitating electrons were approximately uniform over distances of that magnitude.

Experimental electron density profiles obtained with the radar near the time of interest are shown in Figure 3. Results are given for two integration periods of one minute each and for one integration period of 20 sec. All three curves are similar and indicate the electron density profile in the region of radar measurements was fairly stable during the satellite pass near the radar site.

To determine a representative electron flux to apply to the analysis, the particle data were averaged over a four-second interval centered at 1331:09 UT. Figure 4 shows three incident electron flux energy spectra measured by differential energy detectors on the satellite at 1331:09 UT and two seconds before and after this time. Each curve was derived from two sets of detectors. One set was pointing toward the zenith and the other set was pointing 55° away from the zenith. The measured fluxes from the two sets differed by factors of ~ 2 or less.

The three curves in Figure 4 were averaged and the resulting curve was used to represent the incident electron flux during the experiment. The AURORA code was then applied to calculate electron energy deposition rates for a spectrum of this type, assumed to be isotropically incident.

Figure 5 shows the calculated electron density profile resulting from the above primary spectrum. Also shown for comparison is the experimental profile for the time period 1331:00 to 1331:20 UT. A correction has been applied to this curve to account for a small contribution due to an auroral proton component which was

13
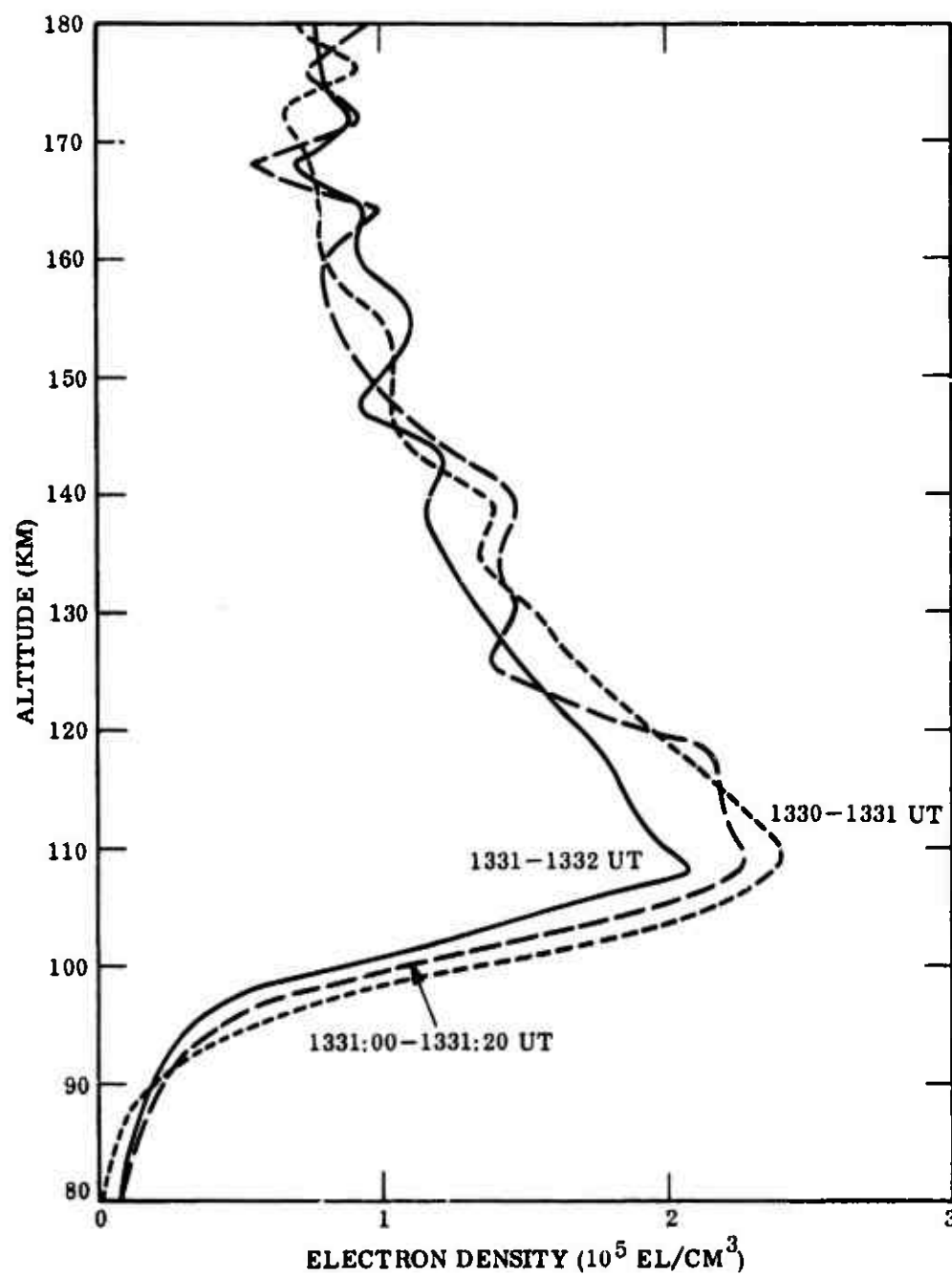
Figure 3. Experimental electron density profiles obtained during the coordinated radar-stellite experiment. Integration periods are indicated.

Figure 4. Incident electron energy spectra determined from particle measurements made on board the satellite during the coordinated radar-satellite experiment.
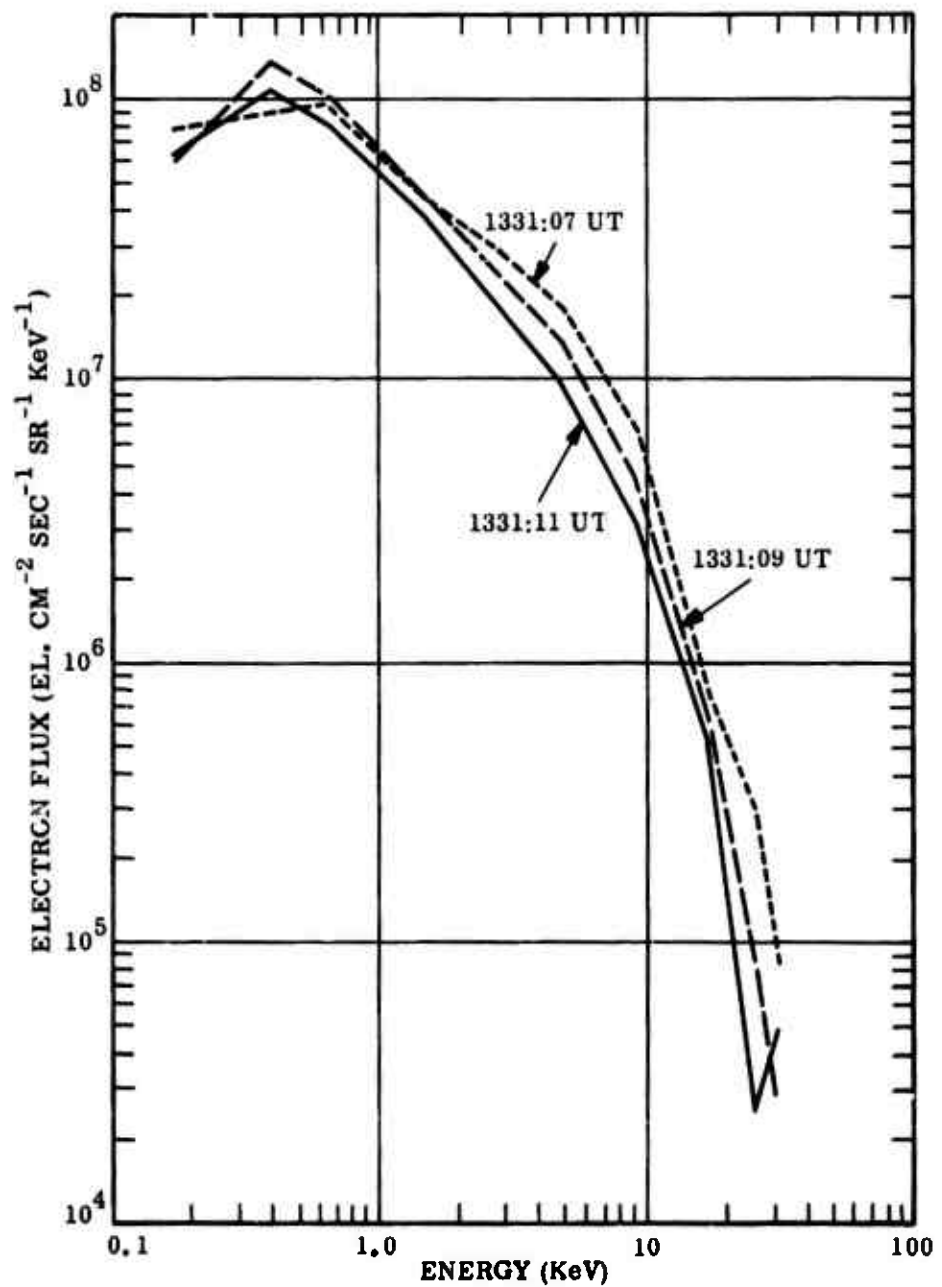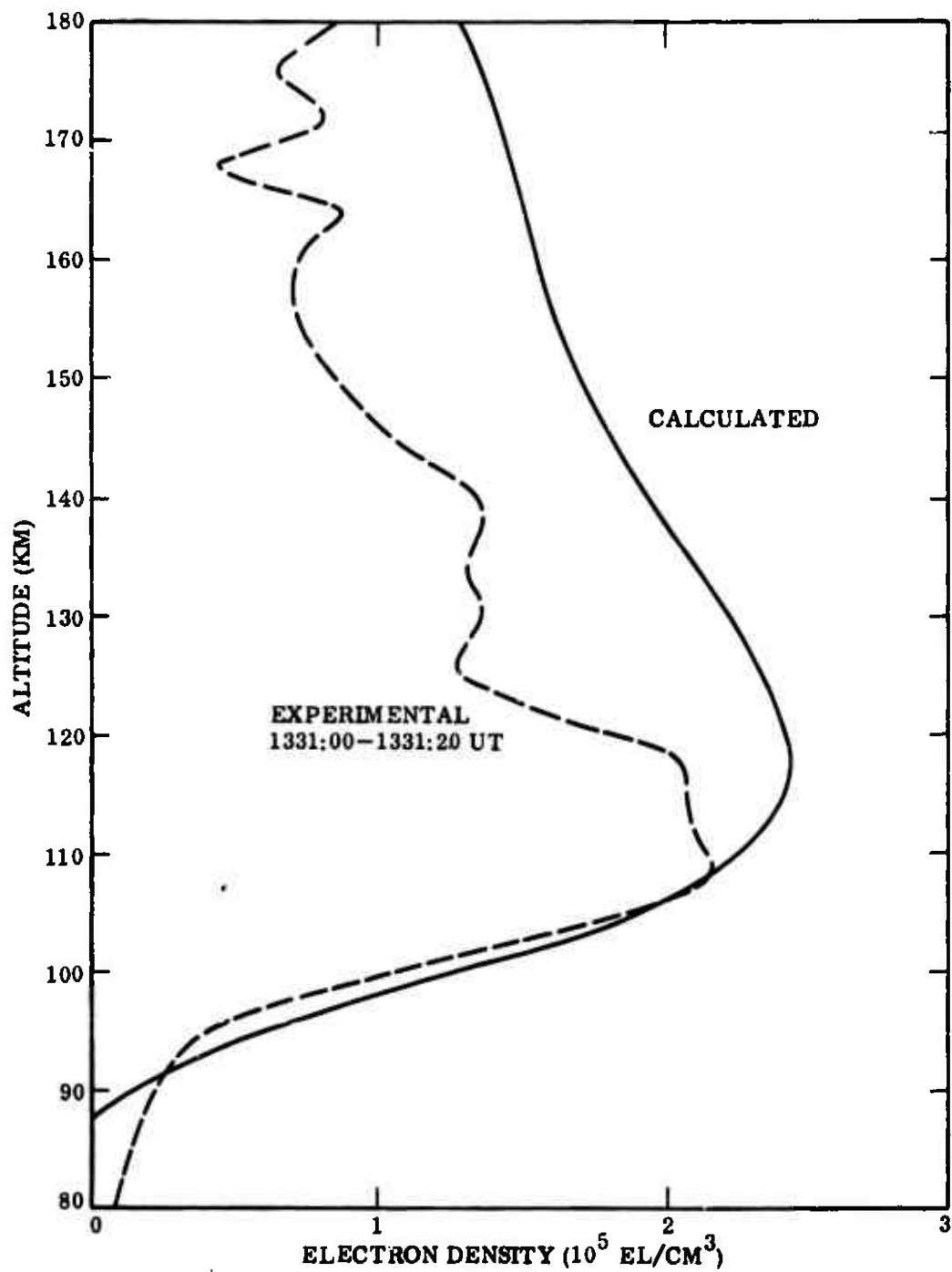
Figure 5. Comparison of experimental and calculated electron density profiles for the coordinated radar-satellite experiment. The experimental profile has been corrected for a small contribution from an auroral proton component.

present during the experiment and detected by proton detectors on the satellite. The correction amounted to less than 10 percent at all altitudes. The procedure for estimating the proton correction is described in Reference 1.

Note that the two curves are in good agreement along the low-altitude edge of the ionization. The peak values are displaced in altitude by several kilometers. At the higher altitudes the calculated density values exceed the experimental values. The discrepancies noted between the curves are large, yet are within the limits of uncertainty introduced by the inaccuracies in particle measurements and the poor radar-satellite geometry.

Because of the large displacement in altitude between the peaks of the two curves, the comparison is less satisfactory for this case than it was for the first case where this particular discrepancy was small. A large fluctuating latitude gradient was observed in the present satellite data, but not in the previous measurements of January 27. Thus the averaged flux used in the present analysis has a larger uncertainty associated with it, which may account for the less favorable comparison between the experimental and theoretical peak positions. The discrepancy may also be due to an accelerating electric field acting on the incident electrons at higher altitudes. Such a field would cause a downward displacement of the observed peak position as discussed in Ref. 1.

We have now analyzed a total of two cases. In both instances, the theoretical and experimental results are consistent with each other, within the uncertainties involved in the analysis. Because these uncertainties are large, additional cases should be investigated to provide a set of results which will lead to a more definite conclusion about the adequacy of the theory incorporated in the AURORA program.

Section 3

APPLICATIONS OF AURORA CODE

3.1 COMPARISON OF ENERGY DEPOSITION CODES

On June 14, 1974, a meeting was held at Lockheed Missiles and Space Co., Inc.
(LMSC) to compare the results of various computer programs which calculate electron
transport in the atmosphere.   In attendance were Major Larry Doan and Dr. Charles
Blank, DNA; Dr. Peter Banks, University of California, San Diego; Dr. Andrew Nagy,
University of Michigan; Dr. Timothy Coffey and Dr. D. J. Strickland, Naval Research
Laboratory; Ellis Hyman, Science Applications, Inc., McLean, Virginia; Nicholas
Winter, Aerospace Corporation; Dr. O. Manley and Dr. Henry Smith, Visidyne, Inc.;
Dr. T. L. Stephens, General Electric-TEMPO; Dr. Douglas Archer and Dr. Paul Tarr,
Mission Research Corporation; and Dr. Martin Walt, Lockheed Palo Alto Research
Laboratory.

Prior to the meeting the input electron fluxes for two sample problems were dis-
tributed to various groups and the individuals were instructed to calculate the
total energy deposit as a function of altitude, the spectrum of the upward and
downward moving electrons at several altitudes, the energy production of various
excited states in atmospheric constituents, and concentrations of selected species
at various times.   Calculations were done by LMSC using a combined LMSC-UCSD code,
Mission Research Corporation (MRC) using the ARTIC program, Naval Research Labor-
atory (NRL), and Visidyne (VIS).   Each of these calculations involved quite different
mathematical methods and approximations.   The NRL code has been revised since the
meeting was held.   The NRL results presented at the meeting are therefore designated
NRL(OLD).   Later results, which are discussed subsequently, are designated NRL(NEW).

18

Comparisons of the results for the total energy deposit as a function of altitude are shown in Figures 6 and 7. Problem 1 consisted of an isotropic input flux at 250 km altitude of the form $f(E) = \exp(-E/10 \text{ kev})$ with a high energy cutoff at 50 kev. Problem 2 involved the experimental spectrum shown in Figure 8. This spectrum of electrons was assumed to be isotropically incident at 200 km altitude along magnetic field lines having a dip angle of 77°. The CIRA 1965 atmosphere was used in both problems.

Although the MRC and LMSC results are in fair agreement with each other, the NRL and Visidyne results are substantially different, particularly for Problem 1. In general the Visidyne curve shows less energy deposited over most altitudes while the NRL results exhibit larger energy deposition at high altitudes and less penetration to extreme ranges.

Drs. Manley and Smith of Visidyne stated that they had inadvertently used a low energy cutoff of 6 kev in their calculations. This cutoff would substantially reduce the input energy and could explain why their energy deposit was less than the other calculations.

A detailed comparison between the NRL and LMSC flux values indicated that the electrons scattered in pitch angle more rapidly with the NRL code. This conclusion was most apparent from the net upward and downward fluxes as calculated by the two methods. Using the NRL-OLD code in Problem 1 the flux at 10 kev was almost isotropic after penetrating to 110 km in contrast to the LMSC code in which the downward flux was about ten times the upward flux. Drs. Strickland and Coffey pointed out that their method of solving the transport equation becomes difficult at high energies and that the scattering treatment might need some modification there.
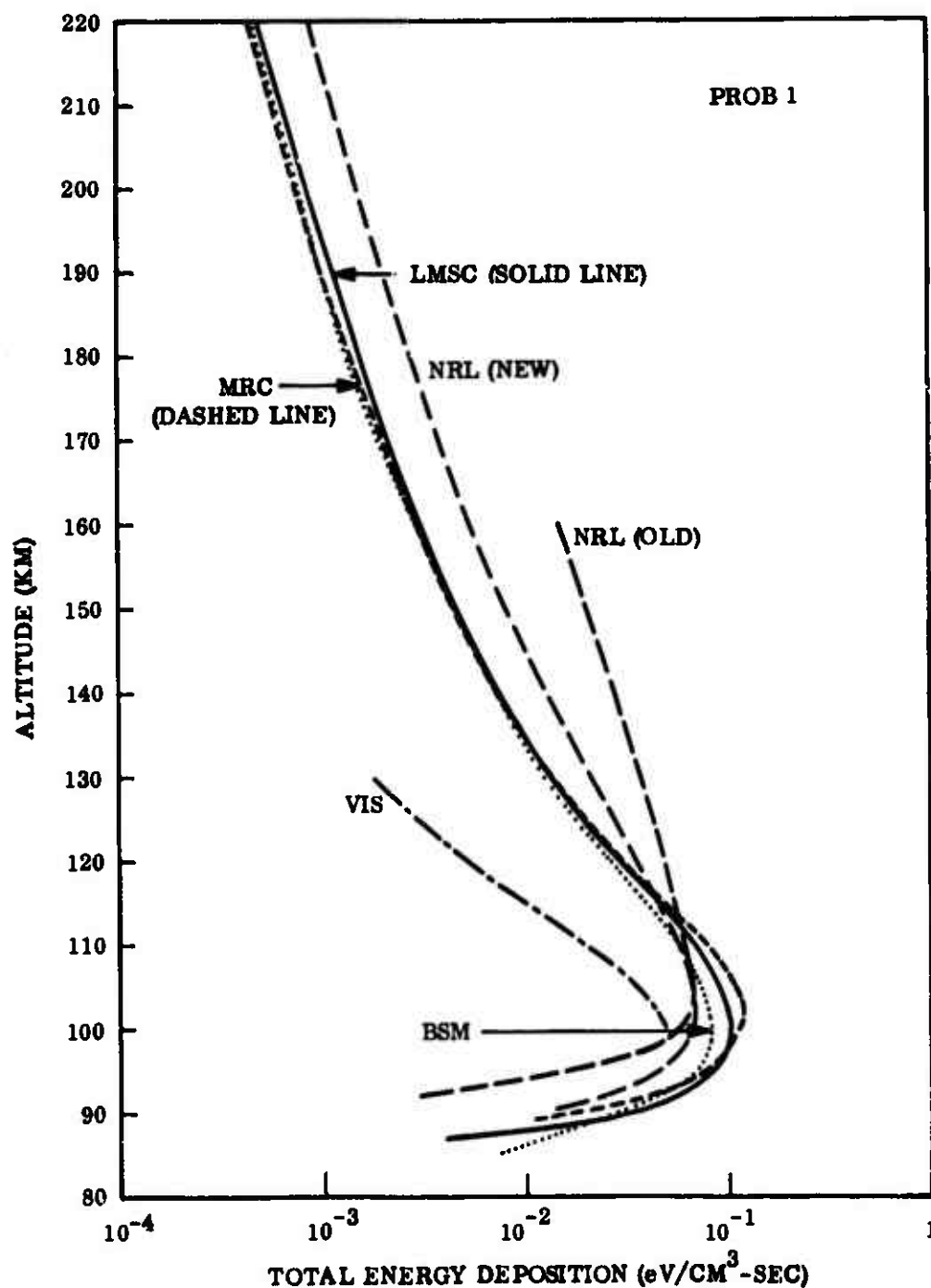
Figure 6. Calculated total energy deposition as a function of altitude for an electron spectrum of the type F(E) = exp (-E/10 keV) isotropically incident at 250 km altitude. Shown are curves obtained by Lockheed Missiles and Space Company, Inc. (LMSC) Mission Research Corporation (MRC), Naval Research Laboratory (NRL), Visidine, Inc. (VIS), and Berger, Seltzer and Maeda (BSM) (Ref. 11).
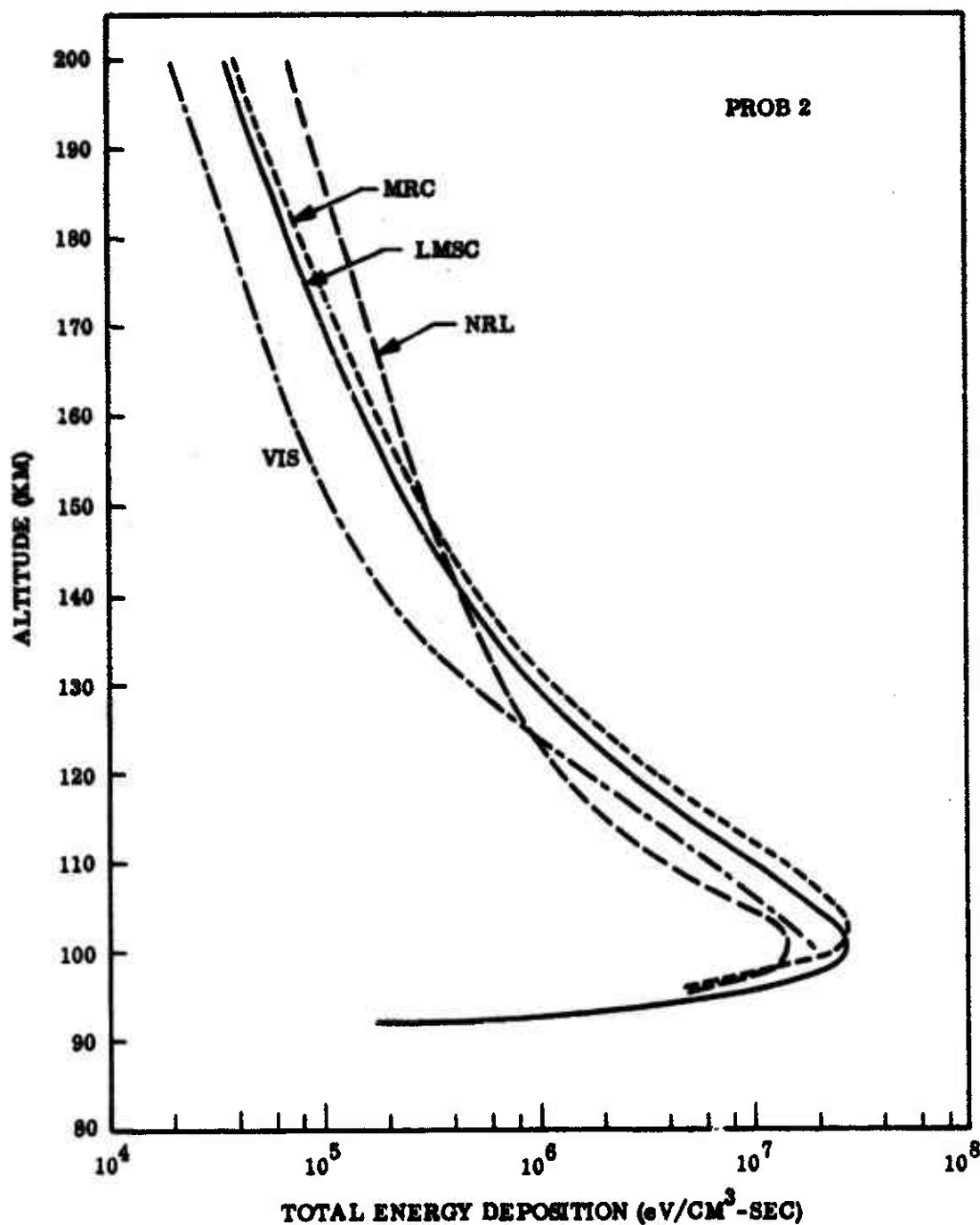
Figure 7. Calculated total energy deposition as a function of altitude for the experimental electron spectrum shown in Figure 8, assumed to be isotropically incident at 200 km altitude along magnetic field lines having a dip angle of 77°. Shown are curves obtained by Lockheed Missiles and Space Company, Inc. (LMSC), Mission Research Corporation (MRC), Naval Research Laboratory (NRL), and Visidyne, Inc. (VIS).

21
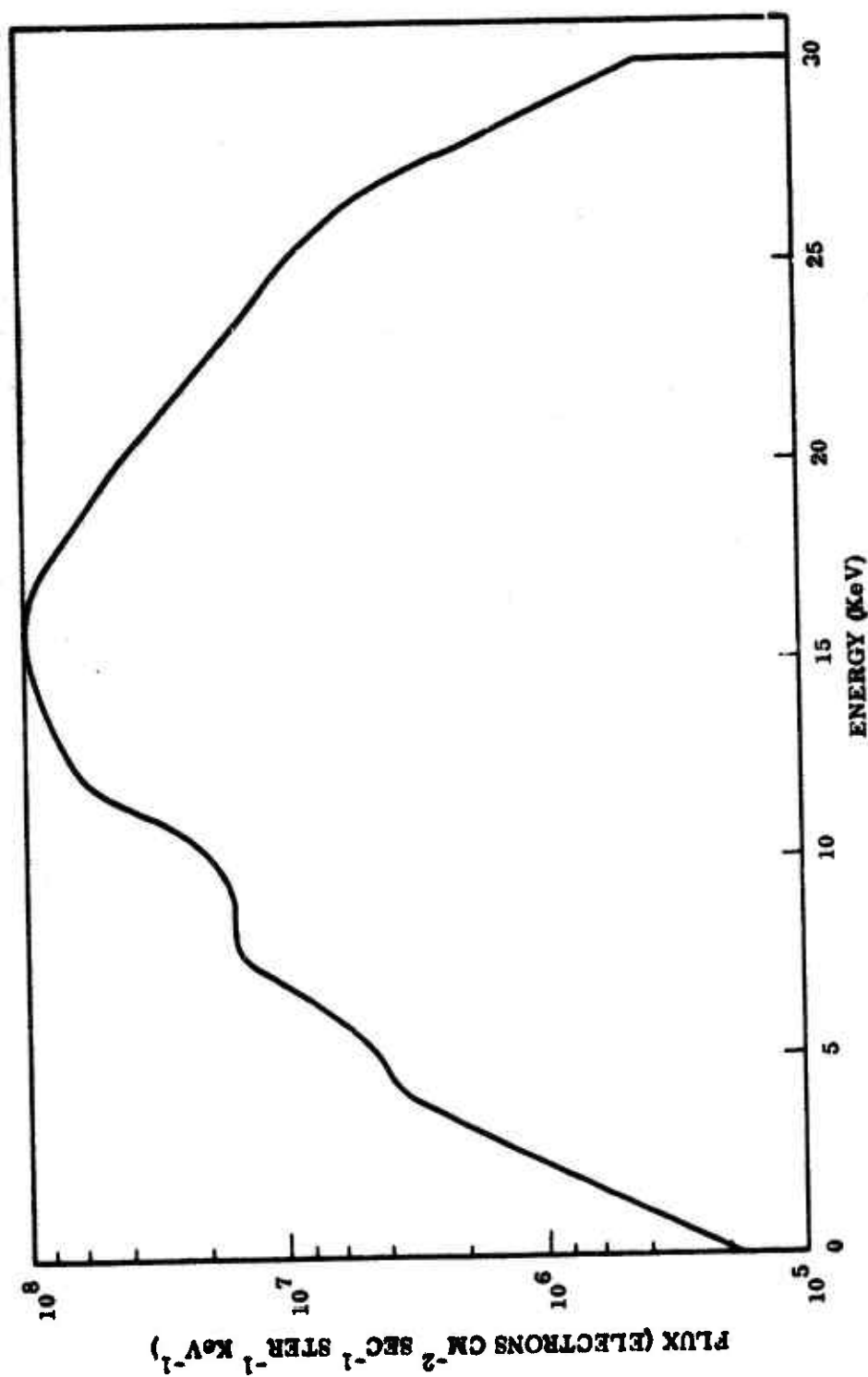
Figure 8. Experimental incident electron flux pertaining to an altitude of 200 km and a magnetic field having a dip angle of 77°.

22

Since the NRL energy deposition and electron fluxes did not agree with those of
MRC and IMSC-UCSD, there was no point in comparing the NRL excitation rates or
chemistry outputs with the other calculations. It was not possible to compare
the upward and downward fluxes of the IMSC-UCSD calculations with MRC since the
MRC ARTIC code did not print out these fluxes. The IMSC-UCSD program normally
calculates excitation rates of major auroral emissions (i.e. 6300 $\overset{o}{A}$, 5577 $\overset{o}{A}$, N_2^+ 2N)
rather than the levels requested by DNA. However, for Problem 2 the code was modi-
fied slightly to give the production rate of the $A^3\Sigma^+$ u state of N_2. This result
was in poor agreement with the MRC result, but the discrepancy was quickly identified
as coming from the use of different sets of Green and Stolarski cross-section
parameters by the MRC and IMSC-UCSD codes.

As mentioned above, subsequent to the meeting the NRL code was modified and rerun
for Problem 1. The new results (unpublished) are designated NRL(NEW) in Figure 6.
Also some results by Berger, Seltzer and Maeda (Reference 11) have appeared that
can be compared with the Problem 1 results. Though their work was not connected
with the DNA-electron deposition codes exercise, one of their cases was identical
with the specifications for Problem 1. The results are labelled BSM in Figure 6.
Berger et al. used an isotropic input spectrum, which was, however, normalized to
a horizontal plane. Their atmospheric model was the same as specified in Problem
1. Berger et al. used a Monte Carlo method which yields relatively precise results
and must take account of scattering at all angles. (The Monte Carlo method leads
to long, tedious computations, and is probably not as suitable as the Fokker-Planck
method (as in AURORA) for DNA's operational requirements.) Comparison of the
results shows that the new NRL calculations still predict slightly higher energy-
deposition values at the higher altitudes although the disagreement is not large.
It is gratifying that three independent calculations, IMSC, MRC, and BSM yield
nearly identical results.

23

3.2 ENERGY DEPOSITION RESULTING FROM HANE

Two computer runs were made with the AURORA computer code to obtain energy deposition results for two HANE problems supplied by Dr. John Ise of General Research Corporation at Santa Barbara, California. The problems involved beta particles produced in a high-altitude nuclear detonation and injected along geomagnetic field lines into the atmosphere. Both problems were identical except for the dip angle made by the field lines, 70.1° (L = 2.9) in one case and 32.3° (L = 1.1) in the other case.

The CIRA atmosphere was used in the calculation. The minimum and maximum energy limits imposed on the calculation were 1 keV and 10 MeV. The incident beta particle spectrum was specified by the formula, $1.36 \times 10^7 \exp(-E)$ $(cm^2\text{-sec-ster-MeV})^{-1}$, where E is in MeV units. This spectrum was assumed to be isotropically incident along magnetic field lines at 150 km altitude. The incident flux crossing a surface perpendicular to the field lines may be easily calculated and is found to be 4.35×10^7 $cm^{-2} \cdot sec^{-1}$ (E > 1 keV). The magnitude of the incident flux corresponds to a realistic situation, and is an estimate of the beta particle flux impacting on the atmosphere at 150 km when a 5-MT nuclear device is detonated at high altitude.

The results of the computer calculations are given in Figure 9, which shows the energy deposition rates as a function of altitude for both problems.

Subsequent to the calculations made by LMSC, results for the same problem in which the magnetic dip angle = 70.1° were also calculated by Dr. Ise, using a General Electric-TEMPO computational model (Ref. 12), and, presumably, the same specified conditions. Electron scattering is ignored in the model, and the reflection of electrons by the converging geomagnetic field is not taken into account. The results are presented as curve B in Figure 10. The corresponding results obtained
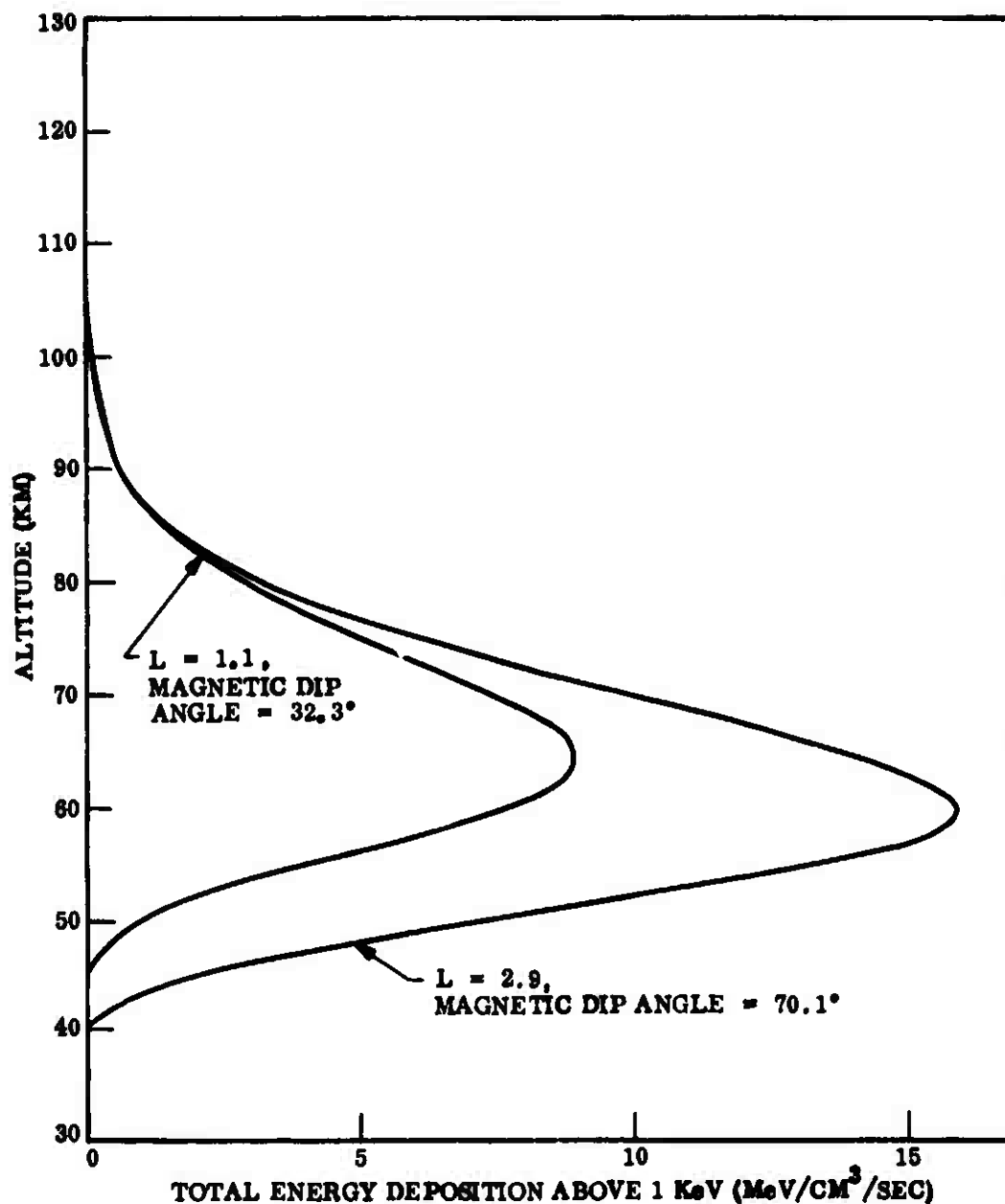
Figure 9. Energy deposited as a function of altitude in the atmosphere by beta particles from two hypothetical high-altitude nuclear detonations, one assumed to occur where the magnetic dip angle = 32.3° and the other assumed to occur where the dip angle = 70.1°. See text for details of the assumed nuclear source.

25
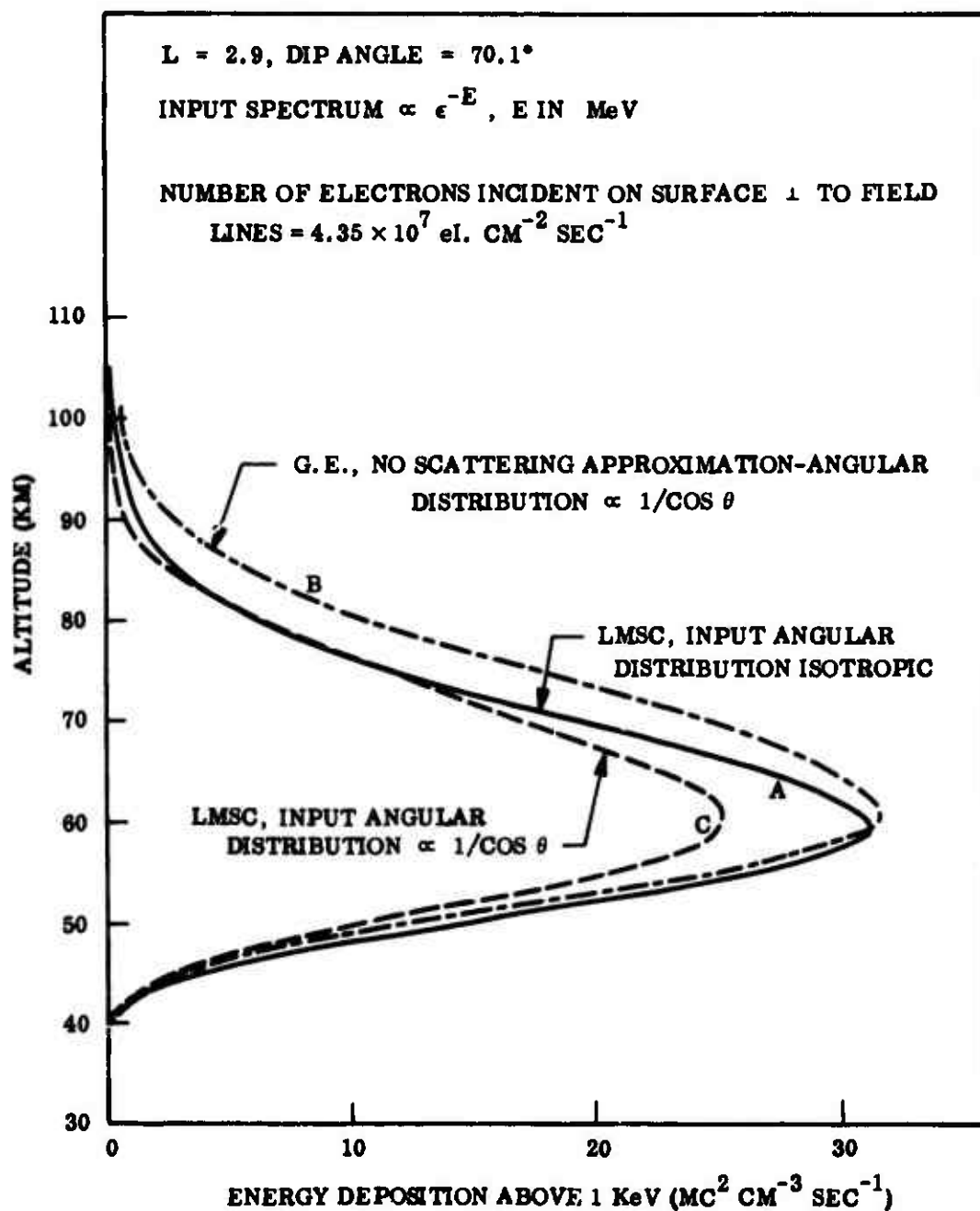
Figure 10. Calculated electron energy deposition as a function of altitude. Curves A and C were obtained by LMSC and curve B was obtained with a General Electric-TEMPO computational model (Ref. 12).

previously for this problem (see Figure 4) by LMSC are given by Curve A. Note the energy deposition is expressed in MeV units in Figure 9 and in Mc^2 units in Figure 10.

A comparison of the two solutions, supposedly obtained for the same problem, indicates discrepancies that are significant enough to require an explanation. In the previous LMSC calculation, the given spectrum of electrons was assumed to be isotropic in pitch angle at the incident altitude of 150 km. However, in the GE-TEMPO formulation of the problem, the pitch angle (θ) distribution of the incident spectrum turned out to be proportional to $1/\cos\theta$ rather than isotropic. (The GE-TEMPO angular distribution is appropriate for a layer of fission fragments located near the top of the atmosphere, while the LMSC angular distribution is better for fission fragments emitting beta particles well above the atmosphere.) Because the GE-TEMPO distribution contains more electrons at large pitch angles, electrons do not penetrate as far, on the average. As a consequence, electron energy is deposited at higher altitudes (curve B) as compared to the results obtained by LMSC (curve A).

To make the comparison more direct, the same problem was run again with the LMSC AURORA code, except that the input angular distribution was made proporational to $1/\cos\theta$ rather than isotropic. Curve C in Figure 10 shows the results of this calculation.

The discrepancies between C and the other curves are attributed to the following. For particles injected at 150 km with a $1/\cos\theta$ distribution, a significant fraction (~20 percent) are reflected by the magnetic field before they penetrate very far into the atmosphere; another fraction (~10 percent) are backscattered. Hence, the total energy loss (given by the integral under the curves) is appreciably less for C than B. The altitude dependence of C is approximately the same as for A because, once the particles penetrate far enough into the atmosphere, their pitch angles are

27

isotropized by scattering. Other differences may result from the approximation

$dE/dx = -2$ MeV/gram cm^{-2} used in the GE-TEMPO code, but are believed to be minor.

4. MODIFICATION OF AURORA CODE

The original version of the low-energy (1 - 500 eV) code that has been incorporated in the AURORA code is described in detail by Banks, et al. (¹ f. 13). This code is based upon solutions to continuity equations which take into account transport of electrons along magnetic field lines as well as the effects of elastic and inelastic collisions with ambient neutral and ionized gases of the upper atmosphere. The Low Energy Auroral Electron Code (LEAURC-I) provides values of upgoing and downgoing hemispherical electron fluxes for energies 1 - 500 eV over a preselected range of altitudes. Starting from a prescribed incident electron flux, the high-energy portion of AURORA computes electron fluxes as a function of pitch angle and altitude for electron energies greater than 500 eV. These results are then trans-mitted to LEAURC-I where the low energy flux computations are made. In addition, LEAURC-I carries out the final calculation of atmospheric auroral emissions and individual species ionization rates using internally generated cross-sections and a standard model atmosphere.

Although LEAURC-I has been applied successfully to practical problems, the code has exhibited several undesirable features. The elimination of these features has led to the development of an advanced version of the code (LEAURC-II) which should prove to be substantially less costly to run while giving more accurate results.

One of the most important changes incorporated into LEAURC-II has been the elimi-nation of all nonessential cross-section calculations. As before, the low energy code obtains the data base (atmospheric densities, electron fluxes, altitude increments, etc.) from the high energy code. Following a short series of internal computations (to include secondary electrons for energies above 500 eV), the low energy code is prepared to begin its computations of the upgoing and downgoing fluxes in the highest energy bin (~ 500 eV). To make these computations, cross

sections for elastic scattering, inelastic scattering, and scattering probabilities are read from a separate cross-section disc-file. In addition, since discrete de-excitation and continuum ionization processes are present, two electron energy transfer matrices are provided to guide the placement of cascading electrons into the proper energy bins. Finally, the various inelastic cross sections for O, O_2 and N_2 are used to compute 38 separate optical excitation rates.

In the earlier version of the low energy code (LEAURC-I), most of the cross-sections were obtained either from analytical approximations to experimental data or tabulated data. Thus, in successive applications of the code, redundant computations were invariably made. The newer version of the code (LEAURC-II) avoids this redundancy through the use of a cross section data file constructed to match the demands of the computational code. Although the use of this file introduces a substantial time-lag between computations of the electron flux in successive energy bins, such a delay does not appear to be a handicap if a multi-processor computer is used.

In addition to its cross-section data file the LEAURC-II code also incorporates an improved energy mesh. Previously, an arbitrary mesh was specified which included a number of discontinuities in the mesh width, ΔE, at selected points. The size of ΔE was chosen to accommodate a fine mesh (~ 1 eV) at low energies ($E < 1$ eV), expanding to a 20 eV width at 500 eV. The fluxes computed with this mesh are regarded as being reasonably accurate but subject to systematic variation near the transition energies where ΔE is abruptly changed. In LEAURC-II a new method of choosing the bin energies has been adopted so that ΔE changes continuously as a function of energy. Although more energy bins are required (and, hence, more computations) a substantial improvement in the computed fluxes should result.

As a final note, during the past year a number of new data have become available for certain excitation and scattering cross-sections. These newer data have been incorporated into the basic data base and should enhance the accuracy of the calculations.

The revised code was used to compute the energy-deposition profile in the atmosphere resulting from the spectrum of precipitating electrons shown in Figure 8 (Test Problem 2). The profile was found to be indistinguishable from the IMSC results shown in Figure 7 at altitudes below about 170 km. Above 170 km the results departed slightly, with the new profile indicating somewhat higher energy deposition.

INTERACTION OF FISSION-DECAY ELECTRONS WITH ION-CYCLOTRON WAVES

5.1 INTRODUCTION

The interaction of relativistic electrons with electromagnetic ion-cyclotron (ion-EMC) waves has been suggested as an important trapped-electron loss mechanism (Ref. 14, Ref. 15), and an important trapping mechanism for artificial rsdistion belts (Ref. 16). The distinction between the two cases is that the trapped electrons can be precipitated while absorbing energy from the ambient waves, but a narrow beam of electrons concentrated in the loss cone is unstable to generation of ion-EMC wavea.

The interaction of electrons with ion-EMC waves may be important whenever an abnormally high number of relativistic electrons is present in the magnetosphere. It could be relevant to the electron precipitation problem and must be examined because it is one mechanism that haa not been included in the AURORA code. In the following section the general theory of wave-particle intersctions in a finite-temperature plasma is discussed. The succeeding section describes a particular instability and its relevance to the artificial electron belt problem and the electron precipitation problem.

5.2 THE FINITE-TEMPERATURE RESONANCE CONDITION

The well-known electromagnetic-mode resonance condition is

$$p_\parallel / m_e = V_\varphi (\gamma - \frac{\Omega_e}{\omega}) \tag{1}$$

where $p_\parallel$ is the component of momentum slong the magnetic field direction, m_e is the electrons' mass, γ is the relativistic "Lorentz" factor, and Ω_e ia the electron

gyrofrequency. The wave is characterized by the frequency ω, which is positive for right-handed (whistler-mode) waves and negative for left-handed (ion-EMC) waves, and the phase velocity, V_φ. The resonance condition with ion-EMC waves is most favorable near the ion gyrofrequency, where simple cold plasma theory gives the dispersion equation

$$V_\varphi \sim c \frac{\sqrt{\Omega_e(\Omega_i+\omega)}}{\Omega_p} \tag{2}$$

where Ω_i is the ion gyrofrequency and Ω_p is the plasma frequency. For ω near $-\Omega_i$ the phase velocity becomes very small, and the resonance condition (Eq. 1) can be satisfied for moderate momenta.

The equation (2) above is, however, not complete. Near the gyrofrequencies the dispersion equation is substantially modified by the effects of plasma temperature. The correct dispersion equation is (Ref. 17, 18, 19)

$$\omega^2(c^2 - V_\varphi{}^2) + V_\varphi{}^2 \sum_{\text{all species}} \omega_p^2 \left[\frac{\omega}{\omega+\Omega_c} + A_T\right]\left[F\left(\frac{\omega+\Omega_c}{\omega} V_\varphi\sqrt{\frac{m}{2T_\parallel}}\right) + A_T\right] = 0 \tag{3}$$

where Ω_c and ω_p refer to the gyro- and plasma-frequency of a particular constituent of the plasma. The so-called temperature anisotropy is $A_T = (\frac{T_\perp}{T_\parallel} - 1)$, and F is defined as

$$F(x) = \frac{x}{\sqrt{\pi}} \int_{-\infty}^{\infty} dy \frac{\exp(-y^2)}{y + x} = - xZ(x) \tag{4}$$

The plasma dispersion function, $Z(x)$ has been tabulated by Fried and Conti (Ref. 20). Near the ions' gyrofrequency the "thermal" part of the distribution predominates, and the anisotropy can be assumed zero.

A slightly simplified dispersion equation can be written in terms of a single Maxwellian tempterature T:

$$\omega(c^2 - V_\varphi^2) + V_\varphi^2 \Sigma \omega_p^2 \frac{1}{\omega+\Omega_c} F\left(\frac{\omega+\Omega_c}{\omega} V_\varphi \sqrt{\frac{m}{2T}}\right) = 0 \tag{5}$$

The temperature must be related to the "beta" of the plasma - the ratio of particle energy to magnetic field energy. We can define three parameters:

$$Q \equiv \frac{\Omega_p^2}{\Omega_e^2} = \frac{N_e m_e c^2}{B^2/4\pi} \tag{6a}$$

$$\beta \equiv \frac{QT}{Rm_i c^2} = \frac{2}{3} \frac{N_i \langle E_i \rangle_{av}}{B^2/8\pi} \tag{6b}$$

$$R \equiv \frac{m_e}{m_i} \approx .000543 \tag{6c}$$

(The definition of β here differs by a factor of $\frac{2}{3}$ from the conventional definition.) Substituting the resonance condition (Eq. 1) in Equation (5), and omitting terms of order ω/Ω_e gives

$$\frac{p_\parallel^2}{m^2 c^2}\left[Q\frac{\omega}{\Omega_e} - RQ\frac{\omega}{\omega+\Omega_i} F\left(\frac{\omega+\Omega_i}{\Omega_e} \frac{p_\parallel}{mc} \sqrt{\frac{Q}{2\beta R}}\right)\right] \simeq 1 \tag{7}$$

Note that in the limit $T \sim 0$, F approaches unity and Equation (7) reduces to the correct approximation

$$\frac{p_\parallel}{mc} \sim \left[\frac{\Omega_e(\omega+\Omega_i)}{Q\omega^2}\right]^{\frac{1}{2}} = \frac{[\Omega_e^3(\omega+\Omega_i)]^{\frac{1}{2}}}{\Omega_p\omega} \tag{8}$$

34

But for finite temperatures, as ω approaches $-\Omega_i$, $F(x)$ is nearly $2x^2$. The resonance/dispersion equation (7) then becomes

$$\left(\frac{p_\parallel}{mc}\right)^4 Q^2 \frac{\omega(\omega+\Omega_i)}{\Omega_e^2 \beta} - \left(\frac{p_\parallel}{mc}\right)^2 Q \frac{\omega}{\Omega_e} + 1 \sim 0 \qquad (9)$$

The quadratic solution is

$$\frac{p_\parallel}{mc} \sim \left[\frac{\beta}{Q} \frac{\omega\Omega_e + \sqrt{\omega^2\Omega_e^2 - 4\omega(\omega+\Omega_i)\Omega_e^2/\beta}}{2\omega(\omega+\Omega_i)}\right]^{1/2} \sim \left[\frac{1}{Q}\left(\frac{\beta\Omega_e}{\omega+\Omega_i} - \frac{\Omega_e}{\omega}\right)\right]^{1/2} \qquad (10)$$

Equations (8) snd (10) tell us that $p_\parallel$ becomes very large as ω approaches either 0 or $-\Omega_i$; we can deduce that there must be a minimum value of $p_\parallel$ for which resonsnce is possible. That minimum should be expected to occur nesr the region where $F(x)$ switches from $2x^2$ to 1, or near

$$x \sim 1 \sim \frac{\omega+\Omega_i}{\Omega_e} \frac{p_\parallel}{mc} \sqrt{\frac{Q}{2\beta R}} \qquad (11)$$

For small values of β, Equations (8) and (11) give

$$\left(\frac{p_\parallel}{mc}\right)_{min} \sim \frac{(2\beta)^{1/6}}{\sqrt{QR}} \sim 43 \frac{\beta^{1/6}}{\sqrt{Q}} \qquad (12)$$

Figure 11 shows the minimum resonant electron momenta (computed from Equation 7), together with the corresponding minimum ion-EMC wave phase velocities (the dimensionless quantity

$$U_{min} = \left(\frac{p_\parallel}{mc} \sqrt{Q}\right)_{min}$$

has been plotted there).

Values of Q are generally of the order 100 inside the plssmasphere and 1 or less outside. Near the plssmapause β may be about 0.1 during moderately disturbed conditions; in that csse the limiting momentum is sbout 1.5 MeV. A reasonable value
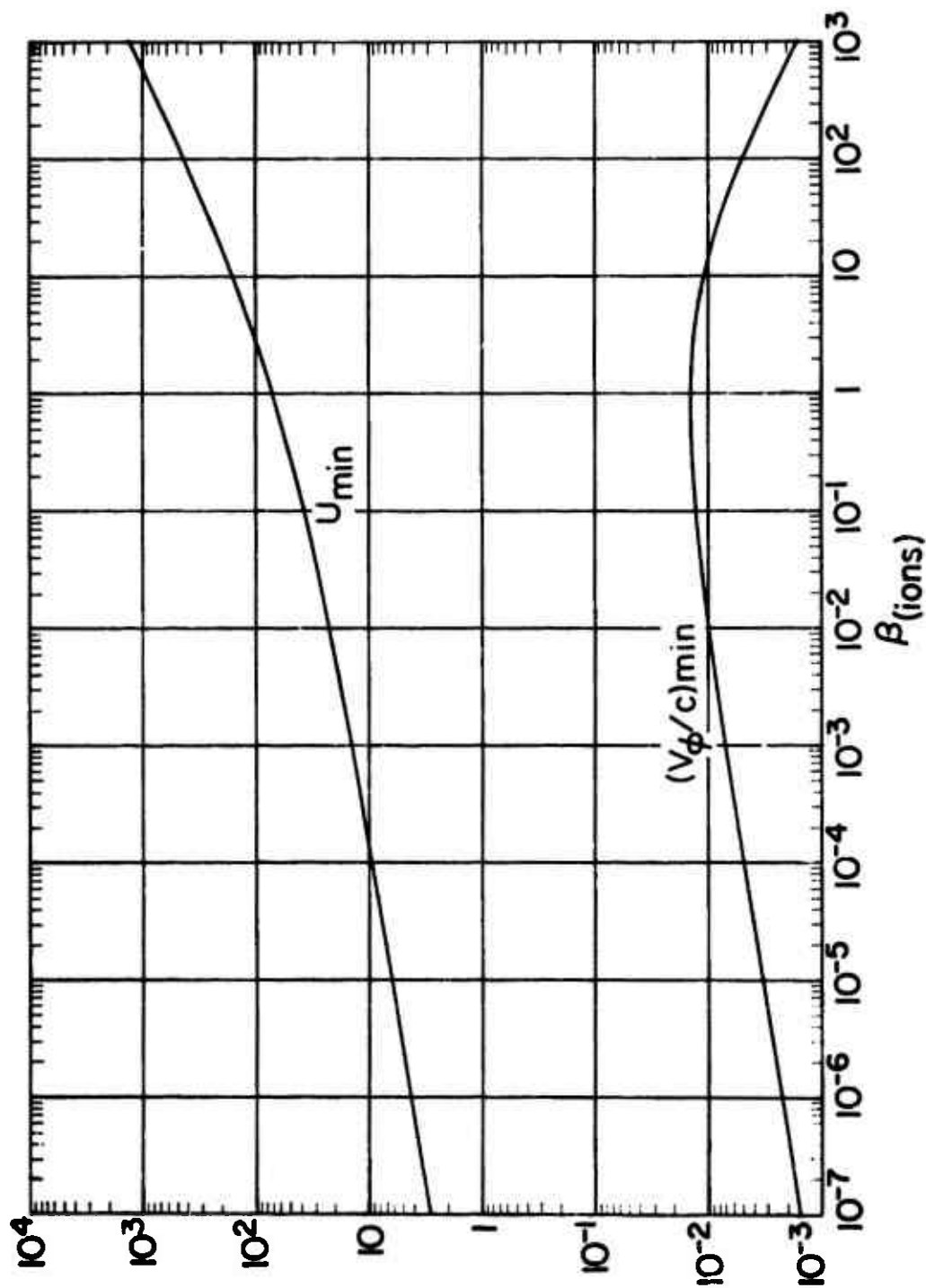
35

Figure 11. The minimum resonant electron momentum and minimum phase velocity for ion-EMC waves related to β.

for β during quiet times right be .001, which gives a limiting resonant momentum of about .7 MeV. The minimum resonant momentum is not very sensitive to β. That the electron momentum has to be at least .7 MeV means that a large percentage of fission-beta electrons might participate in interactions with ion-EMC waves.

5.3 THE AMPLIFICATION OF ION-EMC WAVES BY RELATIVISTIC ELECTRONS

An amplification rate for ion-EMC waves excited by a narrow stream of electrons is readily derived, it is (Ref. 16)

$$Z \equiv \frac{\mathrm{Im}(k)c}{\Omega_e} \cong \frac{p_{\parallel}}{mc} \frac{\pi^2}{2} Q_{Hot} \int_{p_{\parallel}}^{\infty} dp \; p^2 [\frac{1}{2}(1-\mu^2)\frac{\partial f}{\partial \mu} - 2\frac{\omega}{\Omega_e}f]_{\mu \; = \; p_{\parallel}/p} \tag{13}$$

where Q_{Hot} is that part of Q contributed by electrons in the stream. For a stream of electrons concentrated within the loss cone a convenient distribution function is

$$f(\cos \alpha, \; p) = f(\mu, \; p) \approx 3 \; \frac{(\mu_c - \mu^4 - 2\mu_c^2 + 2\mu^2)}{(1 - \mu_c^2)^3} (\frac{m_e}{2\pi T_e})^{3/2} \; \exp(-p^2/2m_e T_e) \tag{14}$$

The amplification rate for that distribution is

$$Z \sim \sqrt{\pi} \; Q_{Hot} \; \frac{p_{\parallel}}{m_e c \; [1+p_{\parallel}^2/m_e^2 c^2]} \left[\frac{p_{\parallel}^2}{2m_e T_e}\right]^{3/2} \exp\left(-p_{\parallel}^2/2m_e T_e\right) \tag{15}$$

Equation (15) represents a continuum spectrum of growing waves, with a well defined fastest growing mode. Numerical solutions for the largest possible value of Z have been constructed, using Equations (7) and (15); the results are plotted in Figure 12. It was necessary to distinguish between the temperatures of the ions and the fast electron stream; in the figure β_c merely denotes the dimensionless product $2QT_c/m_e c^2$ - to be compared with $\beta = 2QT_i/m_e c^2$. The effective temperature of fission-beta
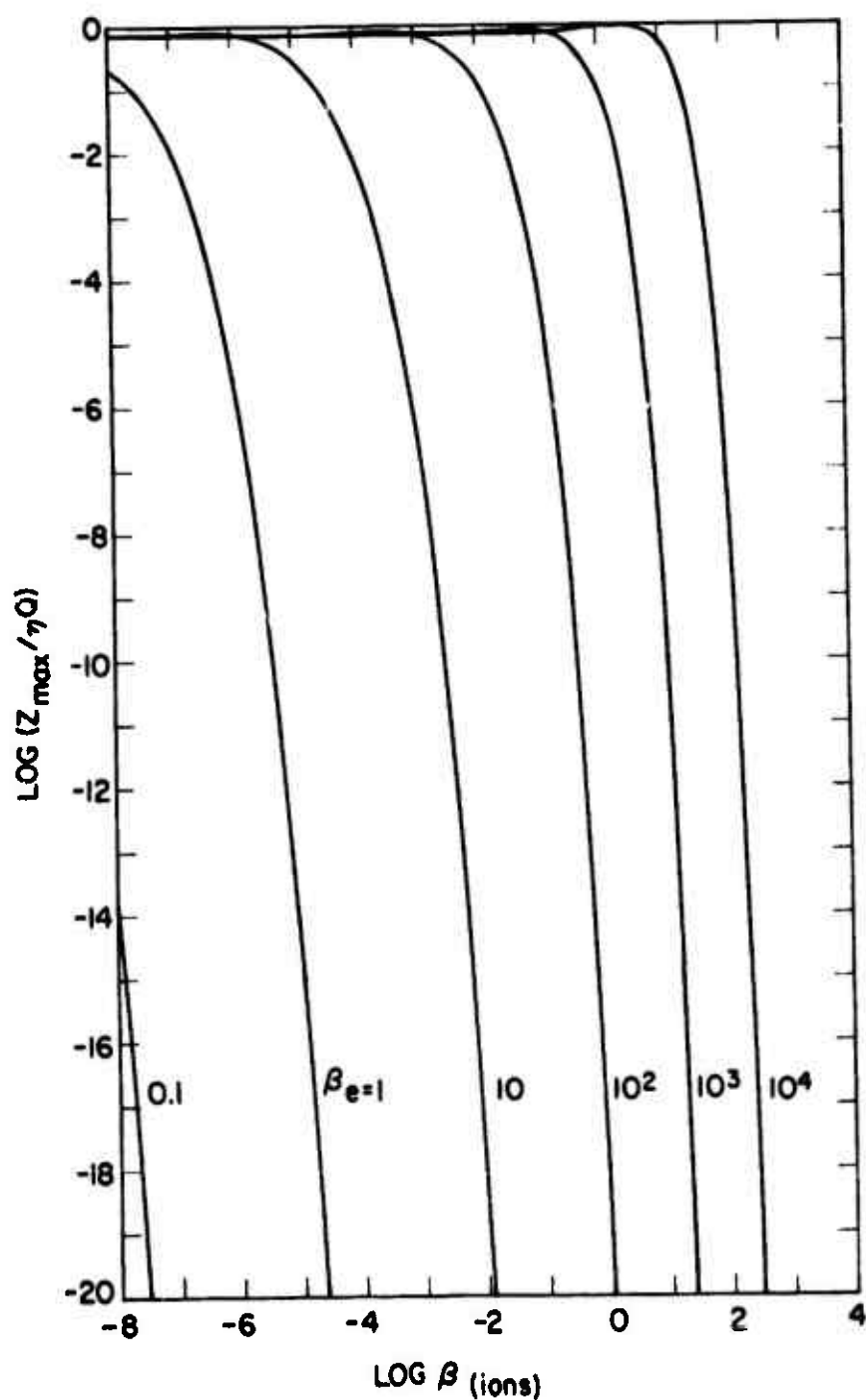
37

Figure 12. Maximum amplification rates for ion-FMC waves excited by relativistic electrons for several values of the electrons' effective temperature, denoted by $\beta_e = 2QT_e/m_ec^2$.

electrons injected by a nuclear explosion is sbout 2 MeV, which leads to a value of about 10^3 for β_e ($Q \approx 100$). For most reasonable values of β the maximum amplification rate is nearly $Z_{max} \sim Q_{Hot}$. Evidently the conditions are generally very favorable to this type of instability.

Of course Q and Q_{Hot} vary along a field line, with a maximum expected near the equator. But the variation in Q_{Hot} is probably not strong, because the density of the electron stream is approximately inversely proportional to B, and therefore compensates for the variation of B in the denominator of Equation (6a). We may suppose that the instability can take place even at rather low altitudes.

The effects of the electron stream-EMC wave instability are easy to imagine. We have the well known conservation of momentum in a reference frame moving with the phase velocity of the wave; expressed as a mathematical formula:

$$p_\perp \delta p_\perp + (p_\parallel - m\gamma V_\varphi)\delta p_\parallel \cong 0 \tag{16}$$

Together with the resonance condition (Eq. 1) this gives

$$\frac{\delta p_\perp^2}{\delta p^2} \cong \frac{\Omega_e}{\omega} \cong -\frac{\Omega_e}{\Omega_i} \approx -2000 \tag{17}$$

Apparently a large change in the transverse momentum, or pitch-angle, is accomplished with a slight expenditure of energy. That the right hand side is negative confirms that a stream of electrons concentrated in the loss cone can give up energy to the waves while being deflected to larger pitch angles. Equation (17) also means that a trapped distribution of relativistic electrons can absorb energy from ion-EMC waves and suffer decreases in their pitch angles.

The mechanism described here can lead to enhancement of artificial trapped electron belts. It could also be an important cause of rapid pitch-angle diffusion in an intense stream of precipitating electrons. The diffusion could take place at a relatively low altitude (above the atmosphere), and must be considered a potential source of error whenever AURORA or other electron energy deposition codes are applied to relativistic electrons.

6. REFERENCES

1. Cladis, J. B., G. T. Davidson, W. E. Francis, L. L. Newkirk, and M. Walt, "Ionospheric Disturbances Affecting Radio Wave Propagation," LMSC/D315887, DNA 3103F, Lockheed Palo Alto Research Laboratory, Palo Alto, California, August, 1973.

2. Leadabrand, R. L., M. J. Baron, J. Petriceks and H. F. Bates, "Chatanika, Alaska Auroral Zone Incoherent Scatter Facility," _Radio Sci._, Vol. 7, p. 747, 1972.

3. Johnson, R. G., J. B. Reagan, and R. D. Sharp, "Satellite Experiments for D-Region Simulation Studies of High-Altitude Nuclear Weapons Effects," LMSC/N-OM-70-1, Lockheed Palo Alto Research Laboratory, Palo Alto, Ca., April 1970.

4. Omholt, A., "The Auroral E-Layer and the Auroral Luminosity," _J. Atmospheric Terrest. Phys._ 7, 73, 1955.

5. Popoff, I. G., R. C. Whitten, R. C. Gunton, J. E. Evans, and E. G. Joki, "Data-Gathering Methods Based on Atmospheric Measurements," _Reaction Rate Handbook_, DNA 1948H, Ed. by M. H. Bortner and T. Baurer, DASIAC, DoD Nuclear Information and Analysis Center, General Electric TEMPO, Santa Barbara, Ca., March 1972.

6. Meyerott, R. E. and J. E. Evans, "Coordinated Measurements of Particles, Luminosity and Electron Concentrations," _Atmospheric Emissions_, Ed. by B. McCormac and A. Omholt, Van Nostrand Reinhold, N. Y., p. 119, 1969.

7. Johnson, R. G., and J. N. Bradbury, "Coordinated Satellite and Ionosonde Measurements During Auroral Proton Events," _Trans. Am. Geophys. Union_, 49, 735, 1968.

8. Jesperson, N, B. Landmark and K. Maseide, "Comparison of Auroral Light Emission and Electron Density," _J. Atmospheric Terrest. Phys._, 31, 1251, 1969.

9. Ulwick, J. C., "Rocket Measurements of Auroral Parameters," _Aurora and Airglow_, B. McCormac Ed., Reinhold, N. Y., p. 225, 1967.

10. McDiarmid, I. B., and E. E. Budzinski, "Angular Distributions and Energy Spectra of Electrons Associated with Auroral Events," Canad. J. Phys., 42, p. 2048, 1964.

11. Berger, M. J., S. M. Seltzer, K. Maeda, "Some New Results on Electron Transport in the Atmosphere," J. Atmospheric Terrest. Phys., 36, 591, 1974.

12. Fischer, P. G., and W. S. Knapp, "Aids for the Study of Electromagnetic Blackout," General Electric-TEMPO, 70 TMP-12, Santa Barbara, Ca., July 1970.

13. Banks, P. M., C. R. Chappell, and A. F. Nagy, "A New Model for the Interaction of Auroral Electrons with the Atmosphere: Spectral Degradation, Backscatter, Optical Emission, and Ionization," J. Geophys. Res., 79, 1459, 1974.

14. Lyons, L. R., and R. M. Thorne, "Parasitic Pitch-Angle Diffusion of Radiation Belt Particles by Ion Cyclotron Waves", J. Geophys. Res., 77, 5608, 1972.

15. Thorne, R. M., and C. T. Kennel, "Relativistic Electron Precipitation During Magnetic Storm Main Phase", J. Geophys. Res., 76, 4446, 1971.

16. Davidson, G. T., "Enhancement of Artificial Electron Belts through Interaction of Electrons with Ion Cyclotron Waves", J. Geophys. Res., 78, 7569, 1973.

17. Cladis, J. B., G. T. Davidson, W. E. Francis, L. L. Newkirk, and M. Walt, "Investigation of Phenomena Affecting Auroral Ionosphere", DNA 3327F (LMSC/ D358493), May, 1974.

18. Davidson, G. T., "Finite Temperature Effects on Pitch-Angle Diffusion of Charged Particles in the Magnetosphere', (Submitted to J. Geophys. Res.).

19. Stix, T. H., "The Theory of Plasma Waves", McGraw-Hill, New York, 1962.

20. Fried, B., and S. D. Conte, The Plasma Dispersion Function, Academic Press, New York, 1961.